

Growth pulsations in symmetric dendritic crystallization in thin polymer blend films

Vincent Ferreiro,^{1,*†} Jack F. Douglas,^{1,*‡} James Warren,² and Alamgir Karim¹

¹*Polymers Division, National Institute of Standards and Technology, Gaithersburg, Maryland 20899*

²*Metallurgy Division, National Institute of Standards and Technology, Gaithersburg, Maryland 20899*

(Received 9 May 2001; revised manuscript received 26 November 2001; published 21 May 2002)

The crystallization of polymeric and metallic materials normally occurs under conditions far from equilibrium, leading to patterns that grow as *propagating waves* into the surrounding unstable fluid medium. The Mullins-Sekerka instability causes these wave fronts to break up into dendritic arms, and we anticipate that the normal modes of the dendrite tips have a significant influence on pattern growth. To check this possibility, we focus on the dendritic growth of polyethylene oxide in a thin-film geometry. This crystalline polymer is mixed with an amorphous polymer (polymethyl-methacrylate) to “*tune*” the morphology and clay was added to nucleate the crystallization. The tips of the main dendrite trunks *pulsate* during growth and the sidebranches, which grow orthogonally to the trunk, pulsate out of phase so that the tip dynamics is governed by a *limit cycle*. The pulsation period P increases sharply with decreasing film thickness L and then vanishes below a critical value $L_c \approx 80$ nm. A change of dendrite morphology accompanies this transition.

DOI: 10.1103/PhysRevE.65.051606

PACS number(s): 81.10.Aj, 47.54.+r, 61.43.Hv

I. INTRODUCTION

The crystallization of polymeric and metallurgical materials under processing conditions normally occurs far from equilibrium and the properties of these materials depend strongly on growth conditions [1,2]. The crystallization front grows as a *propagating wave* into the unstable fluid melt [3] and a wide range of crystal growth patterns can be observed, depending on the extent of undercooling (or supersaturation) and the microscopic structure of the crystallizing species (or rather the symmetries of equilibrium lattice cell). In an early stage of nonequilibrium crystal growth, the orderly pattern of crystallization near equilibrium is characteristically disrupted by the Mullins-Sekerka instability [4–6]. This causes the advancing crystallization front to develop sharp asperities that enhance the local crystallization rate at the expense of the rest of the growing crystal [4–6]. Surface tension acts to moderate the growth of these high surface energy features while the surface tension anisotropy, reflecting the crystal symmetry and orientation, helps to select the symmetry and topological properties of the growing pattern.

The surface tension anisotropy ε specifies the orientational dependence of the surface tension and has been established experimentally and theoretically as a primary parameter governing nonequilibrium crystal growth [3,7]. In two dimensions, ε can be approximately specified by the amplitude of the angle (θ) dependent contribution to the surface tension γ [3,7]

$$\gamma(\theta) = \gamma_0 [1 + \varepsilon \cos(k\theta)], \quad (1)$$

where γ_0 is the isotropic contribution. (Strictly speaking, we should refer to a line tension rather than a surface tension in two dimensions.) The growth of dendrite trunks (main arms

of dendrite) occurs along directions along which $\gamma(\theta)$ has maxima. (This minimizes the surface area in the “exposed directions”.) The periodicity parameter k in Eq. (1) selects the symmetry of the growing crystal, i.e., $k=4$ yields a crystal with fourfold symmetry. In principle, ε can be estimated from measurements of the average tip radius of the growing dendrite crystal, the average crystallization rate, the capillary length, and the diffusion coefficient of the crystallizing molecular species [8,9], and from crystallization near equilibrium [10], but ε has not been measured for high molecular weight polymers (see below). In some systems, anisotropy in the kinetics of molecular attachment to the growing crystal can give rise to anisotropy in the growing crystal that is similar in effect to ε [11]. The growth kinetics anisotropy (usually denoted by β in the literature) is especially important at high rates of crystallization [12]. Anisotropy is necessary for the growth of symmetric dendrites such as snowflakes [3].

The stability and form of the dendrite trunks have a large influence on the ultimate crystallization morphology. For highly supercooled fluids where the rate of crystallization is dominated by the high viscosity of the supercooled liquid (the typical situation for high molecular mass polymeric fluids of crystallizable polymers, such as polyethylene), we often find that the dendrite trunks grow as slender needles [13]. These slender and relatively uniform thickness main dendrite arms exhibit a cascade of branchings to create radially symmetric and space filling structures. The shape of these crystallization patterns is normally circular in thin polymer films and spherical in three dimensions [2,14]. Keith and Padden have suggested that impurities in the crystallizing polymer fluid are responsible for the formation of these structures, as found in the crystallization of certain small molecule fluids with impurities [15,16]. We suspect that stresses in the fluid medium induced by the invasion of the viscous supercooled fluid melt by these *spherulitic* dendrites play a role in the formation of these patterns so that these structures should also occur in pure viscous fluids [13,17]. Further research is needed to understand the origin of this ubiquitous polymer crystallization morphology.

*Corresponding authors.

†Email address: vincent.ferreiro@univ-lille1.fr

‡Email address: jack.douglas@nist.gov

For moderate undercooling, low ε , and modest fluid viscosities, the situation is better understood. The tips of the trunks then tend to split regularly in the center, corresponding to the “doublonic” growth mode [18]. This leads to a somewhat disordered crystallization morphology that has some resemblance to naturally occurring seaweed. This morphology is illustrated below.

At larger values of ε , the tip-splitting phenomenon that characterizes seaweed dendritic growth becomes suppressed and the crystallization morphology is predicted to change into a more *symmetric dendritic crystallization* (SDC) pattern [19]. (The term “symmetric” refers to the number and relative orientation of the dendrite trunks in space.) SDC occurs frequently in the crystallization of small molecule liquids and metals [1,20] and is familiar from our everyday experience with snowflakes and frost. From the beginning of modeling SDC, the highly symmetric appearance of the sidebranches in snowflakes and metallurgical dendrites led researchers to assume that the tip of the dendrite must be unstable to oscillatory modes of boundary deformation that generate the train of sidebranches that characterize dendritic growth [20]. However, careful dendritic growth measurements on succinonitrile symmetric dendrite crystallization gave no evidence for this type of oscillatory growth [21,22]. (Notably these measurement are usually restricted to relatively low undercooling where the thermal noise levels are high.) These experimental findings contradicted an early theoretical treatment of dendritic growth (“geometric model” of crystallization front movement) [23,24] that predicted the *possibility* of oscillatory tip growth, but later models did not yield growth pulsations [24]. The observation of growth pulsations in the “geometric model” is restricted to values of the surface tension anisotropy ε close to a critical value ε_c , where the symmetric dendrites first form, and the model further predicted that the growth oscillations damp to zero for larger values of ε [23]. This model of crystal growth then implies that the observation of pulsating dendritic growth in symmetric dendrites should depend on a particular value of ε . Since ε is normally nearly independent of temperature for a pure material, it is difficult to draw general conclusions about the presence of growth pulsations based on the observation of the crystallization of particular substances. Nevertheless, recent theoretical work [25,26] has emphasized the view, supported by the experimental findings mentioned before, that the amplification of thermal noise is generally the source of sidebranch growth in symmetric dendritic crystallization.

Spontaneous and coherent sidebranching in directional solidification has recently been observed in both experiment and simulation [27–29] and these observations suggest that oscillatory hydrodynamic modes of the dendrite tip can provide an alternative source sidebranch generation in dendritic growth [27–29]. The present paper examines the nature of growth pulsations in SDC crystallization in polymer-blend films where the crystallization rate is much lower than the values normally found in small molecule liquids and metal alloys [1]. Our crystallization measurements correspond to free dendritic growth rather than directional solidification and to a geometry that is nearly two-dimensional.

The use of polymeric fluids to slow down the dynamics of ordering has been exploited in real-space studies of polymer-blend phase separation [30] and this approach allows high resolution measurements of the dynamics of nonequilibrium polymer crystallization using optical microscopy and atomic force microscopy. In the present work, we confine ourselves to investigating the growth of symmetric dendrites in thin polymer-blend films under relatively large undercooling conditions. We employ a polymeric blend of a crystallizable polymer [polyethylene oxide (PEO)] and amorphous polymer [polymethyl methacrylate (PMMA)] that allows us to tune the surface tension anisotropy ε and, thus, the qualitative crystallization morphology [31]. This system should allow us a better chance of observing tip growth pulsations and other dynamical phenomena that might occur near certain critical values of ε , where there are transitions between dendritic growth morphologies.

II. EXPERIMENTAL METHODS

A. Sample preparation

PMMA and PEO materials were purchased from Aldrich [32] and their polydispersity indices k ($k = M_w/M_n$) were determined at NIST by gel permeation chromatography to equal $k(\text{PMMA}) = 1.8$ ($M_w = 7.3 \times 10^3 \text{ g mol}^{-1}$ [32]) and $k(\text{PEO})(M_w = 1.5 \times 10^5 \text{ g mol}^{-1}$ [32]) ≈ 4 . The equilibrium melting temperature T_m of pure PEO was determined to equal $T_m = 338 \text{ K}$ by differential-scanning calorimetry on thick ($20 \mu\text{m}$) evaporated PEO/chloroform films and the glass transition temperatures of the PEO and PMMA films were found to equal $T_g = 213$ and 377 K , respectively. Our estimate of T_m for PEO agrees well with previously reported values [33]. Montmorillonite, “Cloisite” (MON), was supplied by Southern Clay Products [32]. This clay mineral has exchangeable sodium ions, and a cation exchanged capacity of ca. 120 meq per 100 g. One gram of MON and 50 ml of distilled water at 353 K were placed in 100-ml beaker along with 1 g of distearyldimethyl ammonium chloride. The mixture was stirred vigorously for 1 h, and then it was filtered and washed three times with 100 ml of hot water to remove NaCl. After being washed with ethanol (50 ml) to remove any excess of ammonium salt, the product was freeze dried, and kept in a vacuum oven at room temperature for 24 h. The resulting organically modified montmorillonite (OMON) dispersed well in chloroform, although the unmodified MON did not do disperse well in the polymer-blend spin-casting solution.

The blend components were dissolved in chloroform at a concentration between 0.3% and 3% relative weight of the polymer to solvent, unless otherwise stated. Thin blend films of this solution were then spin coated onto Si substrates [Semiconductor Processing Co. [32], orientation (100), Type P] at a spin speed of 2000 rpm. This procedure results in films of uniform thickness between 100 and 500 nm. Isothermal crystallization was made by heating the films at 377 K for 10 min (above the melting temperature) and then cooled down quickly (50 K/min) to the desired crystallization temperature (see caption of Fig. 1 for specifications of crystallization temperatures in our measurements). Prior to spin coat-

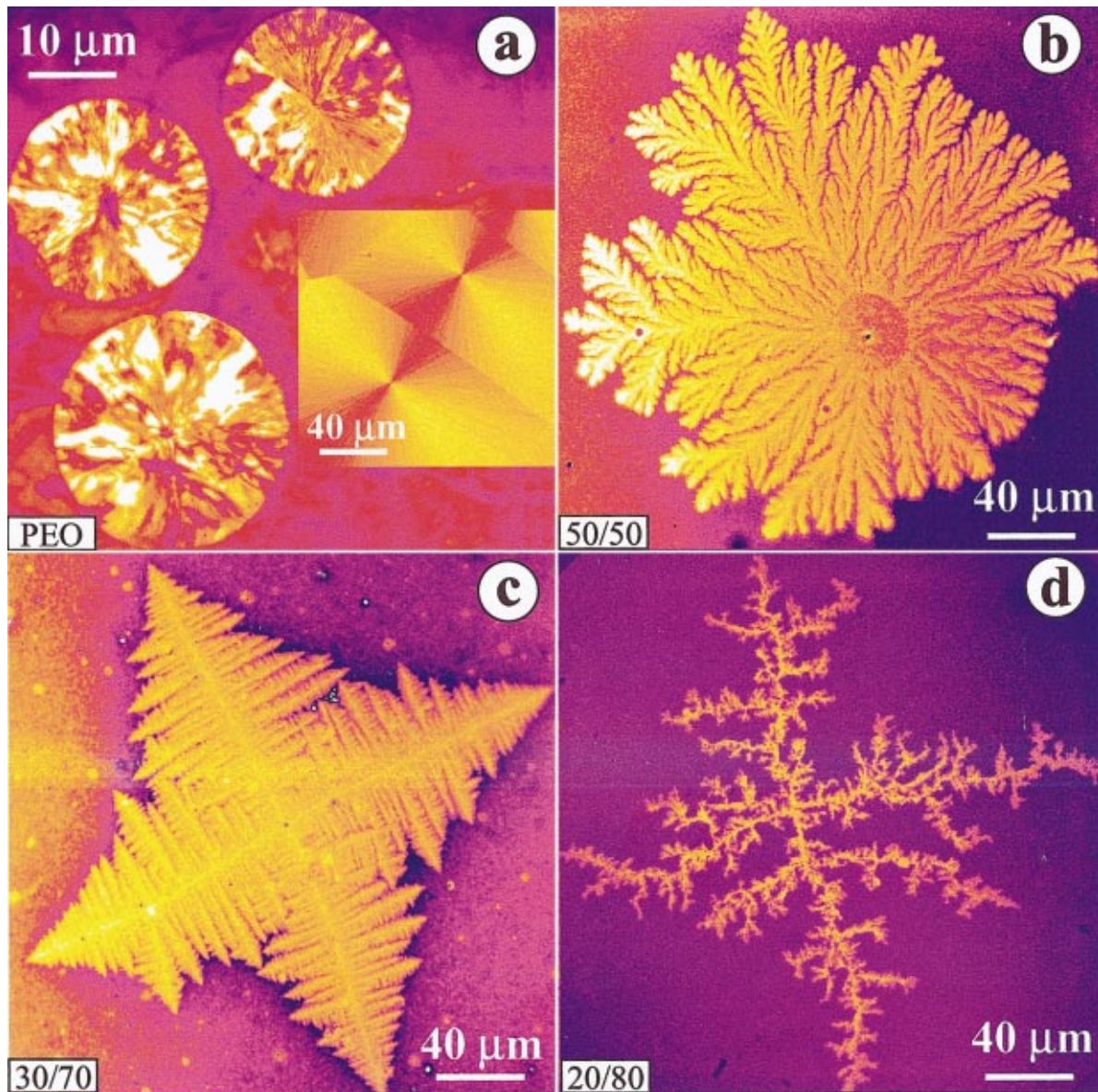


FIG. 1. (Color) Polymer crystallization morphologies as a function of polymer composition. The relative clay polymer mass has been fixed at 5% (OM images rendered in false color). (a) Spherulitic crystallization of a film of pure PEO ($T_m = 340$ K, $\delta T = 0.09$). (b) Seaweed dendritic growth in a (50/50) PEO-PMMA film ($T_m = 332$ K, $\delta T = 0.07$). (c) Symmetric dendritic growth in a (30/70) PEO-PMMA film. (d) Fractal dendritic growth pattern in a (20/80) PEO-PMMA film. T_m was determined by differential scanning calorimetry on 20- μm -thick evaporated films.

ing, the polished Si substrates were treated for 2 h with a solution of 70% H_2SO_4 /30% H_2O_2 at 353 K and then rinsed with de-ionized water.

There have been several previous studies of blends of PEO and PMMA, encompassing mixtures of components of various molecular weights, and this blend is usually indicated to be miscible over a wide temperature range [33–35]. However, lower critical solution temperature (LCST) phase separation has been reported in PEO-PMMA films for temperatures below the critical temperature of about 623 K [36,37]. The as-cast films have the appearance of a phase separation morphology that presumably formed during the film drying [38] and we find a smoothing of this surface topographical structure for temperatures above a

temperature-composition locus that resembles a UCST cloud point curve [38]. By studying the temperature dependence of this smoothing we estimated the UCST critical composition ϕ_c and critical temperature, $\phi_c \approx 0.55$ and $T_c \approx 378$ K [38]. Previous determinations of cloud point curves of relatively thick PEO/PMMA polymer films cast from chloroform indicate $T_c = 365$ K and $\phi_c = 0.53$ for a PEO-PMMA blend having molecular masses of $M_{w \text{ PEO}} = 4 \times 10^4$ and $M_{w \text{ PMMA}} = 10^5$ g mol $^{-1}$ [32] and $T_c = 381$ K and $\phi_c = 0.62$ for molecular masses of $M_{w \text{ PEO}} = 10^6$ and $M_{w \text{ PMMA}} = 10^6$ g mol $^{-1}$ [32,39].

It should be appreciated that the residual solvent in the spun-cast film probably influences the phase separation behavior that we observe and we can also expect the solvent to

“plasticize” the film (i.e., modify the dynamics of the film related to the glass transition of PMMA, leading to increased molecular mobility in these viscous films). Although the residual solvent effect complicates the determination of temperature range where phase separation occurs, it should not change the qualitative nature of the crystallization phenomenon under investigation. The thermodynamics and general aspects of phase separation and crystallization in monotectic mixtures (two liquids and one solid phase) are discussed by Cahn [40].

B. Measurement methods

Reflective optical images were obtained with an optical microscope (OM) using a Nikon optical microscope [32] with a digital Kodak MegaPlus, charge-coupled device camera attachment [32]. We follow the growth kinetics of the patterns using automated data acquisition with a resolution of 1024×1024 pixels.

All the atomic force microscopy (AFM) experiments were carried out in air by using a Dimension 3100 microscope from Digital Instruments operating in the Tapping mode™ [32]. In this mode, the cantilever is forced to oscillate at a frequency close to its resonance frequency with an adjustable amplitude. The tip, attached to the cantilever, was a pure silicon single crystal tip (model TSEP) with a radius of curvature of about 10 nm. The tip contacts briefly the film surface at each low position of the cantilever and the amplitude of the oscillation varies. “Height” images are obtained by using the feedback loop that keeps the amplitude at a constant value by translating vertically the sample with the piezoelectric scanner: height measurements are deduced from those displacements. For the engagement we used a ratio $A_{sp}/A_0=0.9$, where A_0 is the free oscillation amplitude and A_{sp} the set-point one [41]. The (512×512 pixels) images have been obtained by using a ($100 \times 100 \mu\text{m}^2$) piezoelectric scanner; the scanning frequency was 0.5 Hz and the mean value of the repulsive normal force was 0.1 nN. All the “height” images have been filtered through the “Planefit” procedure [41]. We also used the AFM to measure the thickness of the film scratching the surface or masking a border of the wafer before spin casting the solution. The vertical resolution of AFM is 0.1 Å.

III. RELATED BLEND FILM MEASUREMENTS

In an earlier work, we investigated the real space structure of (amorphous) polymer-blend phase separation by forming nearly two-dimensional polymer films in which one of the polymer components segregates to both the solid substrate and the polymer-air boundary [30]. These “ultrathin” films were also restricted to film thickness range in which phase separation occurs within the plane of the blend film [30]. The difference in the surface tension between the blend components causes the film to buckle in response to phase separation within the film [30]. This buckling provides a good source of contrast in optical and AFM measurements, enabling high-resolution measurements of the dynamics of the ordering process in real space. Here we extend this earlier work by incorporating a model crystallizable polymer (PEO)

into the film to study dendritic growth. We mix PEO with an amorphous polymer (PMMA), which is the component that segregates to the film boundaries. Clay particles are added as nucleating centers for the PEO crystallization. The clay particles are convenient because they induce centrosymmetric crystallization patterns. Crystallization can also be induced by scratching or piercing the film with a sharp implement so these particles are not essential for inducing crystallization.

Tunable crystallization morphology

The crystallization morphology of PEO mixed with PMMA in a thin-film geometry can be “tuned” through spherulitic, seaweed, symmetric dendritic, and fractal dendritic patterns through the adjustment of the PMMA composition. These crystallization morphologies are described in a separate paper [31] and here we briefly review the essential nature of this phenomenon before specializing our discussion to the growth of symmetric dendrites. In Fig. 1 we illustrate changes in the crystallization morphology of PEO/PMMA blend films arising from a variation in the polymer composition. Crystallization was performed at 305 K and the clay concentration of the spin-casting solution was fixed at 5% of the mass of the blend. The PEO melting temperature T_m depends on the polymer composition and T_m values are indicated in the caption, along with the undercooling, $\delta T = (T_m - T_{\text{crys}})/T_m$. Clay particles can be seen at the center of the patterns shown in Fig. 1, confirming that the clay acts as a nucleating agent. Over a large range of PEO mass fraction (50–100 % of PEO by mass), we find circularly symmetric spherulites [Fig. 1(b)]. This is the “normal” polymer crystallization morphology encountered under processing conditions [1,2,14–16]. In the insert of Fig. 1(a), we show the late-stage spherulitic crystallization morphology where the spherulites impinge on each other and deform to form a domain wall morphology similar in appearance to a Voronoi cell pattern [42]. The sidebranching of the spherulite “needles” becomes increasingly coarse with the increasing PMMA composition in this concentration regime [31], but the spherulites tend to retain their nearly circular shape. At an almost 50/50 polymer blend (PEO/PMMA) mass ratio, we find a regime [Fig. 1(b)] where the spherulite morphology changes into a *seaweed dendrite* morphology [19]. This morphology exhibits broad growing tips that split intermittently and one of the newly formed branches normally grows to predominate over the other. The dominant branch (“alpha branch”) then splits again and the process repeats itself. Tip splitting is the dominant feature of seaweed dendritic growth and this morphology is well known from recent modeling of nonequilibrium crystallization (see below) and has been confirmed in many experimental studies. Increasing the PMMA concentration further to near 30/70 leads to another dramatic change in the polymer crystallization morphology. In Fig. 1(c), we observe well-formed *symmetric dendrites* where the fourfold symmetry of equilibrium PEO crystallization asserts itself at a macroscopic scale [43]. The solution and the melt grown crystals have the same crystal structure (square-shaped crystals) under near-equilibrium conditions [43]. (We have observed nearly square crystals in our films when

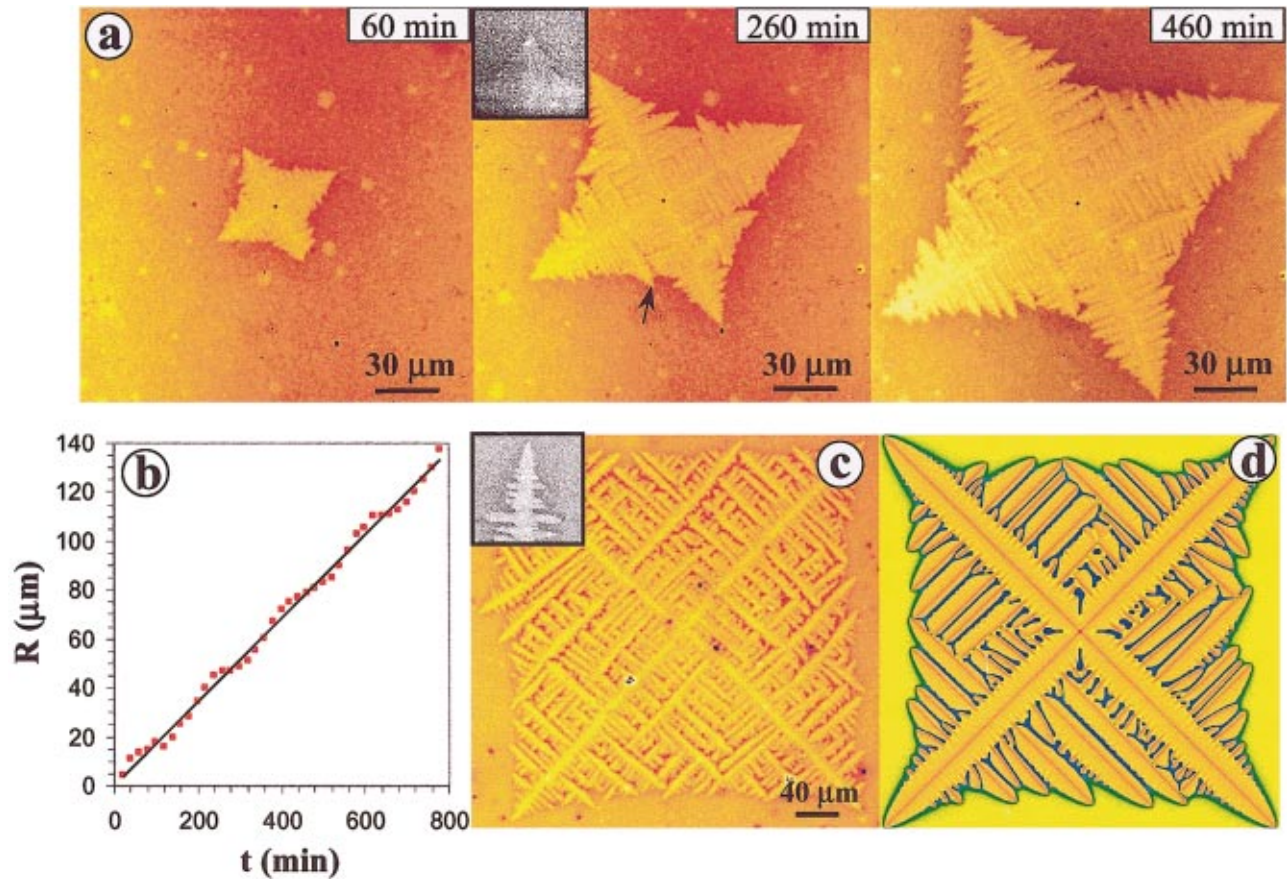


FIG. 2. (Color) Growth of symmetric dendrites in a crystalline amorphous polymer blend film. (a) Symmetric dendritic growth occurs for a 30/70 relative PEO/PMMA mass concentration blend and a 5% relative mass concentration of clay to polymer. The degree of undercooling is $\delta T = 0.10$. We show (false color) optical images of a symmetric polymer dendrite for 60, 260, and 460 min and the pattern at 800 min is shown as an inset in Fig. 6. The inset in the 260 min optical image shows a higher resolution AFM image of the dendrite tip. The lateral dimensions of the AFM image are $20 \times 20 \mu\text{m}^2$ and z range = 40 nm. The pixel resolution for this AFM picture is 40 nm. (b) The distance of a dendrite trunk tip from the center of the dendrite $R(t)$ (μm) (clay particle seeds are black dots in the images) as a function of time t (min). The arm length is measured by optical microscopy with a resolution of 1024×1024 pixels using $100\times$ objective. For the optical microscope images the pixel resolution is equal to $0.2 \mu\text{m}$. The uncertainties for the data of (d) are less than the size of the data points. Note oscillatory growth. This oscillatory phenomenon has also been confirmed from AFM pictures recorded as a function of time. (c) Symmetric polymer dendritic growth in a near two-dimensional polymer film resolved by an optical microscope (objective $100\times$). The inset shows a topographical AFM image of the dendrite tip region. The dimensions of the “height” AFM image are $20 \times 20 \mu\text{m}^2$ and z range = 30 nm. For this picture the pixel resolution is 40 nm. (See Fig. 8 for the AFM pictures recorded as a function of time.) (d) Phase field simulation of symmetric dendritic growth in a Ni-Cu alloy (see text for growth conditions). Note resemblance to the two-dimensional polymer dendrites in (c).

we crystallize at 331 K near T_m .) Note the near registry of the sidebranches on each side of the growing dendrite arm and the uniformity of the “starlike” envelope curve describing the positions of the sidebranch tips of the dendrite. Symmetric dendritic polymer crystallization patterns have often been observed in polymer crystals grown on surfaces from polymer solutions [44], but we are unaware of previous observations of SDC in melt blends. (However, distorted spherulitic and randomly branched crystallization morphologies have been observed in melt blends [45].)

At still higher concentrations of PMMA (20/80), we observe another morphological transition from the symmetric dendritic crystallization to the highly branched, fractal morphology illustrated in Fig. 1(d) [31]. This interesting transition is not well understood yet, but we do note that the high concentration of PMMA makes the film highly viscous and

this could have an impact on the stability of the dendrite tips and the gross crystallization morphology. It is also notable that the growth should be diffusion-limited in this regime and the low concentration of PEO could also contribute to the noisy nature of the resulting crystal growth in this regime. In the following, we focus specifically on the dynamics of symmetric dendrite crystallization, corresponding to relative PEO/PMMA-mass concentration of 30/70 and 5% clay by mass, relative to the polymer.

IV. OBSERVATION OF SYMMETRIC POLYMER DENDRITE CRYSTALLIZATION IN A BLEND FILM

Figures 2(a)–2(d) show optical images (false color) of the growth of a (PEO-rich) symmetric dendrite over a sequence of times from 60 to 460 min. The film thickness is 160 nm

and the dimensionless undercooling $\delta T = (T_m - T_c)/T_m$ equals 0.01. Note the cusplike shape of the envelope curve describing the tip positions of the dendrite arms, a feature observed previously in symmetric dendrite growth at relatively high undercooling [46]. The sidebranches of the dendrite in Fig. 2(a) grow nearly perpendicularly to the slender and nearly parabolic main branch of the dendrite. Our dendritic crystallization images were acquired at a rate of one picture every 5 min and in Fig. 2(b) we show the increase in the tip position from the center of the dendrite. (The clay seed at the dendrite center is the noticeable dark spot at the center of the dendrite.) We observe that the tip position of the dendrite grows in an *oscillatory* manner about an average constant rate $R_o = 0.171 \mu\text{m}/\text{min}$. The period P of the tip growth oscillations is of the order of 100 min.

It is important to realize that the dendrite morphology changes in thinner films. Figure 2(c) shows an example of dendritic growth in a 50-nm-thick film, where the crystallization conditions (temperature, composition) are the same as in Fig. 2(a). (This morphological transition is discussed below.) Notably, the dendrite in Fig. 2(c) *does not* exhibit growth pulsations and has a more disordered appearance and its boundary envelope has a squarelike shape. The inset in Fig. 2(c) shows an AFM image of the dendrite tip region, showing again a similarity to the form in the AFM and optical images. Despite differences in the large-scale crystallization morphology, the tip radius in Fig. 2(c) is nearly the same as in Fig. 2(a), ($r \approx 1 \mu\text{m}$). The AFM data is discussed quantitatively below.

We obtain some insight into these dendritic growth patterns by comparing to phase field simulations of two-dimensional SDC in a two-dimensional fluid mixture [47]. The simulation in Fig. 2(d) corresponds to a Ni-Cu alloy ($\phi_{\text{Ni}} = 0.59$), where ε is taken to have a relatively large value, $\varepsilon = 0.05$ and δT is relatively large for metallurgical fluids, $\delta T = 0.013$. (The new phase field calculation in Fig. 2(d) is for $\varepsilon = 0.05$, which is larger than the ε considered in previous work [47] ($\varepsilon = 0.04$), but otherwise the model parameters are identical to those specified in Ref. [47].) Comparison of the simulation to our measurements is meant to be only qualitative. The main point is that growth pulsations are *not observed* in the two-dimensional phase field simulation, but we do find a reasonable resemblance between the “two-dimensional” polymer dendritic growth shown in Fig. 2(c) and the simulated crystallization patterns [Fig. 2(d)]. Apparently, no ε measurements have ever been made on high molecular weight polymers, and at present we are restricted to qualitative comparisons between the phase field model and our measurements.

The oscillations in the tip radius in Fig. 2(b) are quantified by subtracting the *average dendrite tip radius* $\mathfrak{R}(t) = R_o t$ [straight line in Fig. 2(b)] from $R(t)$. Figure 3(a) shows that the *tip position fluctuation* $\delta R(t) = R(t) - \mathfrak{R}(t)$ is nearly sinusoidal; the solid curves correspond to a fit of $\delta R(t)$ to $\delta A_R \sin(2\pi t/P)$, where δA_R is the *oscillation amplitude* and P is the *pulsation period*. We next compare $\delta R(t)$ to a measure of fluctuations in the width $\delta w(t)$ of the dendrite arm. To determine the dendrite sidebranch width $w(t)$ we choose an *arbitrary* sidebranch [denoted by arrow in Fig. 2(a)] and

define $\delta w(t)$ as the orthogonal distance from the tip of the sidebranch to the center line of the main dendrite arm. The sidebranch width grows with an average rate (equal to R_o to within experimental uncertainty) with oscillations $\delta w(t)$ about this average. Our determination of $\delta w(t)$ in Fig. 3(a) shows that $\delta w(t)$ oscillates *out of phase* with $\delta R(t)$. Further, a “phase plot” of $\delta R(t)$ versus $\delta w(t)$ in Fig. 3(b) reveals that the dendritic growth in Fig. 3(a) is governed by a *limit cycle* with a phase angle α difference of about 164° (see caption of Fig. 3).

The dendritic growth in Fig. 2(a) has a self-similar appearance and this suggests that it might be useful to determine the apparent mass-scaling dimension (fractal dimension) describing the symmetric polymer dendritic growth. The determination of fractal dimension d_f was determined from image analysis based on the area-perimeter technique [48]. In Fig. 4(a), we show a plot of the polymer dendrite area A and perimeter p obtained by digitizing the optical image series corresponding to the dendrite growth shown in Fig. 1(a). We observe that a power law relation $A \sim p^{1/d_f}$, can fit fairly well the data and we determine d_f from the slope of $\log p$ versus $\log A$. This gives an apparent fractal dimension $d_f = 1.78 \pm 0.05$, where the correlation coefficient for the power law fit is $R^2 = 0.98$. Notably, we do not observe growth pulsations in Fig. 4(a) so that A and $p^{1/1.78}$ must exhibit similar growth oscillations. The near linearity of the plot in Fig. 4(a) confirms the impression of the near self-similarity of the polymer dendritic growth pattern.

The temperature dependence of the rate of dendritic growth for a $L = 160 \text{ nm}$ film is shown in Fig. 4(b) as a function of undercooling, $\Delta T = (T_m - T_c)$. Over the temperature range investigated, the rate of crystallization R_0 can be described by a power law, $R_0 \sim (\Delta T)^\delta$ where $\delta \approx 2.53 \pm 0.02$. The correlation coefficient for the power law fit is $R^2 = 0.99$. A power scaling of R_0 with an effective exponent near 2.6 has been suggested to be a “universal” property of dendritic growth in small molecule liquids [49].

Since theory offers limited guidance about the factors governing the period P of dendrite growth pulsations, we explore the influence of some obvious system parameters under our control—undercooling, polymer composition (supersaturation) and film thickness, L . In Fig. 5(a) we show $\delta R(t)$ for a range of undercooling $\Delta T = (T_m - T_c)$ values in the range (288–308 K). Apparently, P has no appreciable dependence on ΔT , but Fig. 5(b) shows that δA_R increases nearly exponentially with ΔT . The correlation coefficient for the exponential fit is $R^2 = 0.99$. A change in the relative polymer composition has a large influence on the pulsation rate, but this effect can cause a *qualitative* change in the crystallization morphology [31] so we restrict ourselves to a composition range where the SDC is observed. A decrease of the PMMA concentration causes a decrease in p and an increase in δA_R for a fixed $\Delta T = 35 \text{ K}$, (e.g., $P \approx 105 \text{ min}$ and $\delta A_R \approx 15 \mu\text{m}$ for a 35/65 blend while $P \approx 180 \text{ min}$ and $\delta A_R \approx 9 \mu\text{m}$ for a 30/70 blend). We next explore the change in the growth pattern dynamics and morphology associated with reducing the film’s thickness.

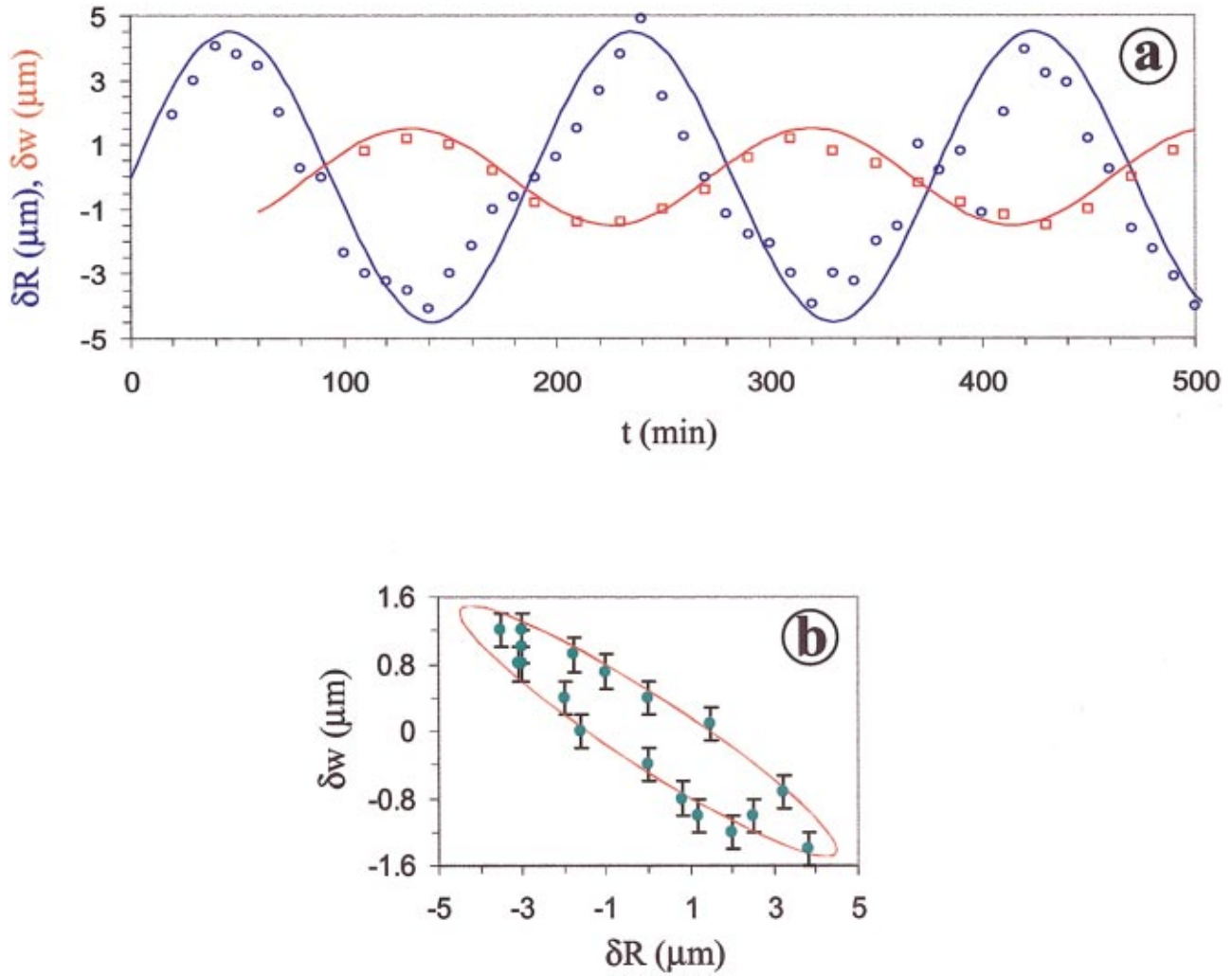


FIG. 3. (Color) Fluctuations in the position of the tip and sidebranch width. (a) Fluctuations in the trunk tip position $\delta R(t)$ and sidebranch positions $\delta w(t)$. \circ and \square denote $\delta R(t)$ and $\delta w(t)$ data, respectively. See text for definitions of $\delta R(t)$ and $\delta w(t)$. (b) “Phase plot” of $\delta R(t)$ vs $\delta w(t)$, which shows a limit cycle oscillation in these coordinates. From the data fit the phase angle is estimated to equal $\alpha = 164^\circ \pm 4^\circ$. The correlation coefficient for the fit is $R^2 = 0.97$. The fits correspond to $\delta R(t) \approx \delta A_R \sin(2\pi t/P)$ and $\delta w(t) \approx \delta A_w \sin(2\pi t/P + \alpha)$, where δA_R and δA_w are amplitudes and α is a phase angle difference.

Figure 6 shows that P first *increases* sharply with *decreasing* film thickness L , but then *drops precipitously to zero* below a critical film thickness, $L_c \approx 80$ nm. The SDC is similar to Fig. 1(a) for $L > L_c$, but we observe a different morphology for $L < L_c$ (see Fig. 2(c) and inset to Fig. 6). Thus, we have direct evidence that the morphological transition is accompanied by a change in the dynamics of the dendrite tip. The lack of pulsations in the “two-dimensional” blend film dendrites is also reflected in the extent of correlation in the position of the sidebranches on each side of the primary growing parabolic dendrite arms [see Fig. 2(c)]. The registry of sidebranches and the cusplike envelope curve describing the positions of the sidebranch tips in the symmetric dendrite shown in Fig. 2(a) are contrasted with the “two-dimensional” dendrite ($L < L_c$) shown in Fig. 2(c). There is little correlation in the sidebranch positions on either side of this dendrite. This enhanced regularity of structure in the

pulsing dendrite is reminiscent of the regular sidebranching found in the growth of dendritic growth subjected to periodic external perturbations [50,51]. We, therefore, suggest that the oscillatory tip mode imparts regularity to the growing dendrite.

Finally, we should mention in this section that oscillatory growth front modes have recently been reported in the spherulite and seaweed crystallization morphologies for other materials (Fig. 1; see Discussion) so that the presence of hydrodynamic modes in propagating crystallization fronts appears to be a general, but nonuniversal, phenomenon. However, the study of the dynamics of these other nonequilibrium crystallization morphologies will require the development of specialized measurement techniques for each morphology (the splitting of the dendrite tip creates some ambiguity in defining the precise location of the crystallization front), so in the present paper, we confine our attention to symmetric dendrite growth.

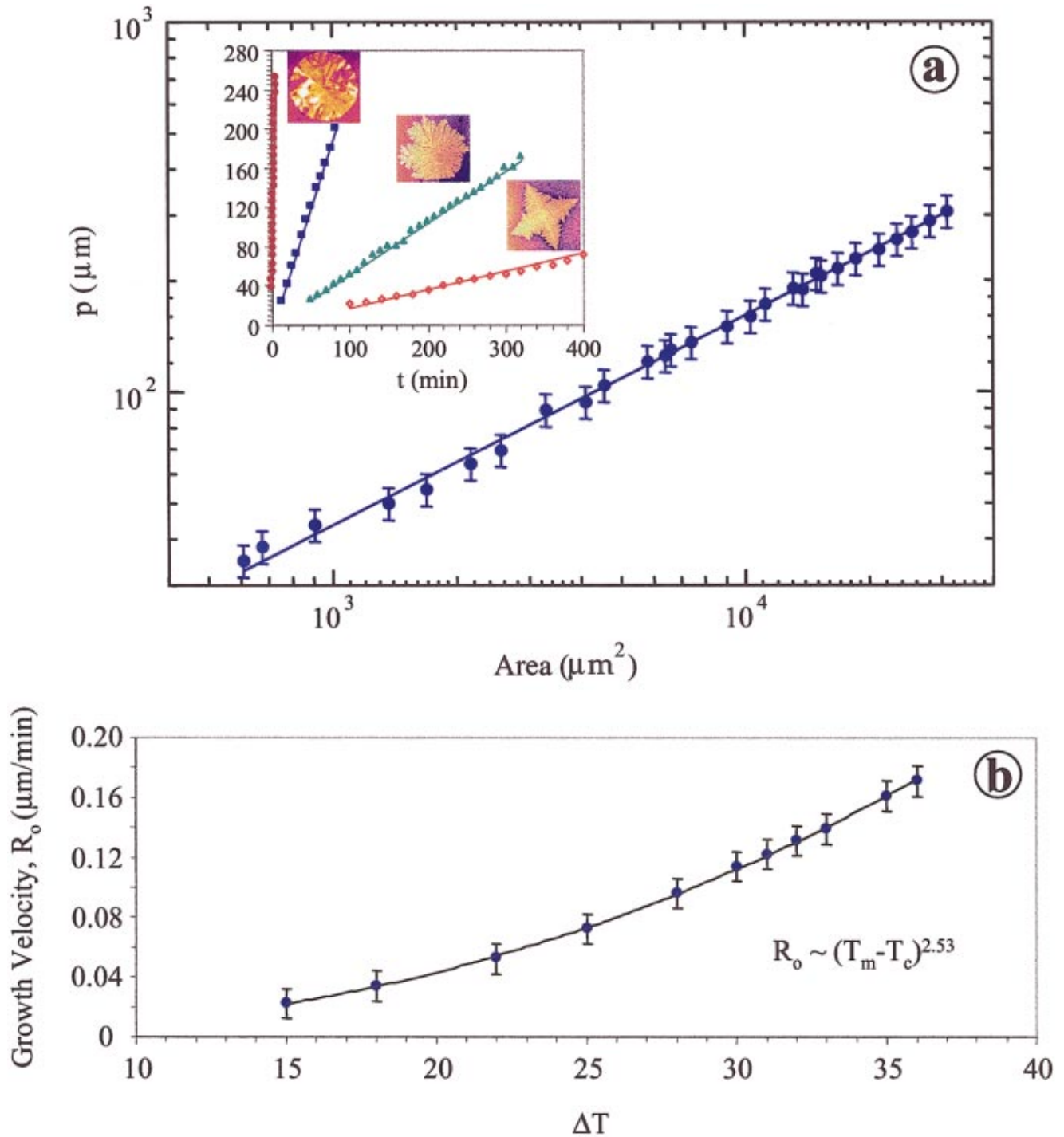


FIG. 4. (Color) Kinetics of polymer dendritic growth. (a) The dendrite perimeter p vs area A determines an apparent fractal dimension of the growing dendrites. The data points denote observations based on a figure of the growth of the dendrite shown in Fig. 2(a). The inset denotes the average tip velocity for the morphologies shown in Fig. 1 for a fixed degree of undercooling, $\delta T=0.07$ (●, pure PEO spherulites; ■, 60:40 spherulites; ▲, 50/50 seaweed dendrite; ◇, 30/70 symmetric dendrite). (b) The average rate of crystallization for (30/70) symmetric dendrite $L=160$ nm films as a function of undercooling $\Delta T=(T_m-T_c)$.

V. MORPHOLOGICAL TRANSITIONS IN SYMMETRIC POLYMER DENDRITIC GROWTH

The singular nature of the shift in P with L provides an important clue into the nature of the dendritic growth pulsa-

tions. At first, we anticipated that P would correspond to a diffusion-controlled depletion time that would scale quadratically with film thickness. This expectation would lead to a decrease of P with film thickness; an effect *opposite* to our measurements. We then realized that the L dependence of P

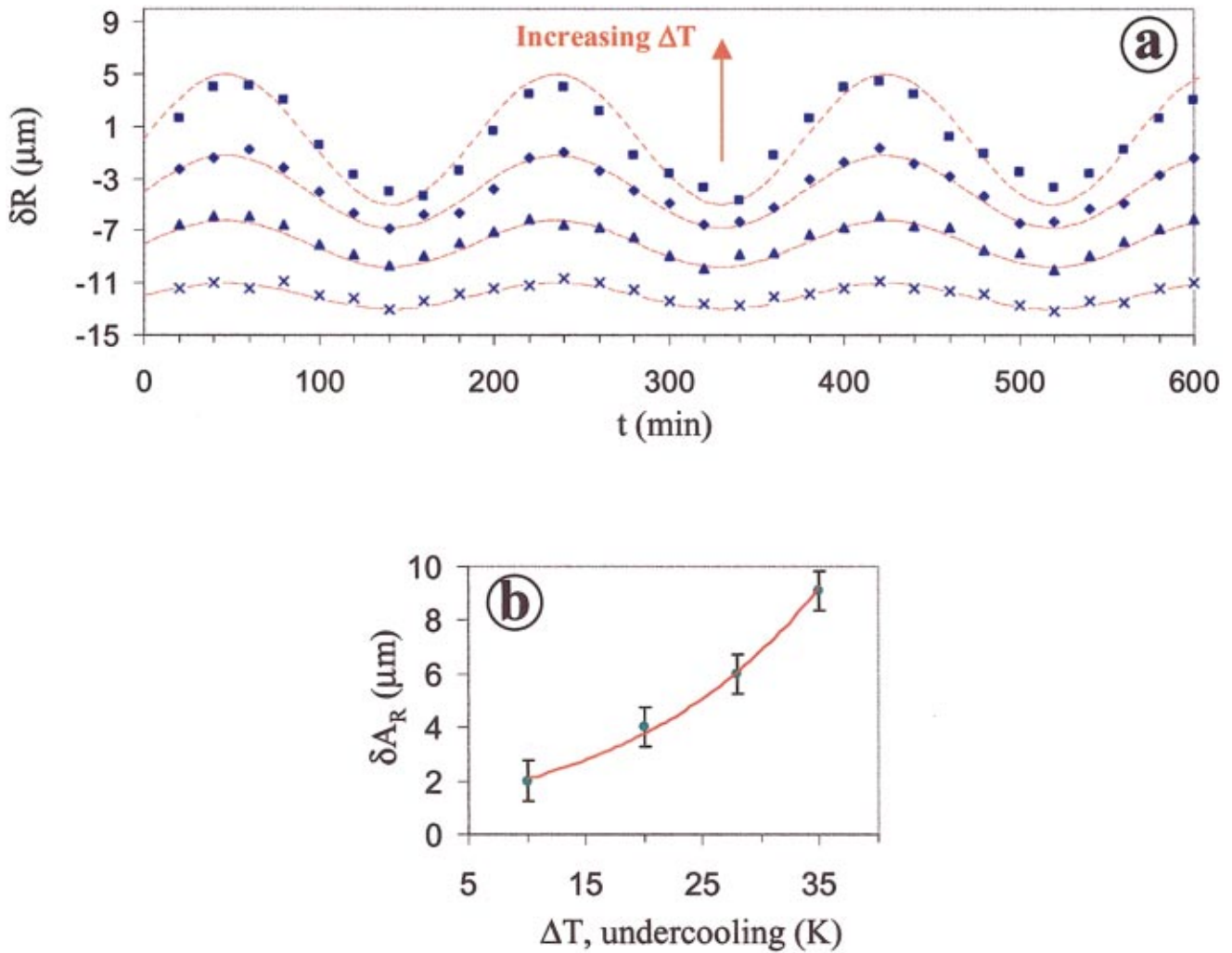


FIG. 5. (Color) Influence of the degree of undercooling on tip pulsation. (a) Fluctuations in the tip position $\delta R(t)$ as a function of undercooling, \blacksquare , \blacklozenge , \blacktriangle , and \bullet denote $\delta T = 0.1, 0.08, 0.06,$ and 0.03 , respectively. Curves have been offset by a constant (time average of δR equals 0) so that the curves do not overlap. (b) Amplitude δA_R as a function of undercooling. The amplitude grows nearly exponentially with undercooling. The correlation coefficient for the exponential fit is $R^2 = 0.99$.

is similar to the finite-size dependence of pulsations observed in oscillatory chemical reactions. This comparison is natural because Belousov-Zhabotinsky (BZ) reactions also exhibit pattern formation with propagating wave fronts. The oscillation period of the BZ reaction occurring in ion-exchange beads [52] (which causes the color of the beads to flicker) likewise increases strongly with decreasing bead radius and the oscillations *cease* when the bead size became smaller than a critical radius (0.2 mm). In Fig. 6, we compare our measurements of P to the functional form suggested by the studies of finite-size effects on the BZ reaction (bead radius is replaced by polymer film thickness) [52]. This leads to the relation, $P = P_\infty / (1 - L/L_c)$ for $L > L_c$, $P_\infty = 90$ min and $P = 0$ for $L < L_c$. The correlation coefficient for the data point fit is $R^2 = 0.99$. The finite-size dependence of the oscillation period in the BZ reaction was attributed in Ref. [51] to a change in the reaction rate due to the inactive nature of the reaction at the bead surface, leading to a correction of the reaction rate involving the surface-volume ratio. In our own measurements, the boundaries of the blend film are enriched

in PMMA so that a similar finite-size effect on the pulsation period is plausible.

The viewpoint of a supercooled liquid as a variety of the excitable medium and crystallization as a variety of reaction-diffusion wave propagation also gives insight into the influence of the clay particles on the crystallization morphology. At low concentrations, the clay particles mainly serve as centers of the dendritic growth and similar dendritic patterns can be obtained by punching or scratching the film without clay. The “catalyst” particles play a similar role as an excitation source for BZ reactions in solutions loaded with ferroin-loaded resin beads [53]. As is well known, the BZ reaction in a fluid layer gives rise to symmetric “target” chemical waves at low bead concentrations, but these patterns break up into rotating spiral patterns at higher bead concentrations due to the interference between the chemical waves [53–55]. Our proposed analogy between nonequilibrium crystallization and autocatalytic chemical reactions would lead us to expect a similar symmetry breaking phenomenon in dendritic crys-

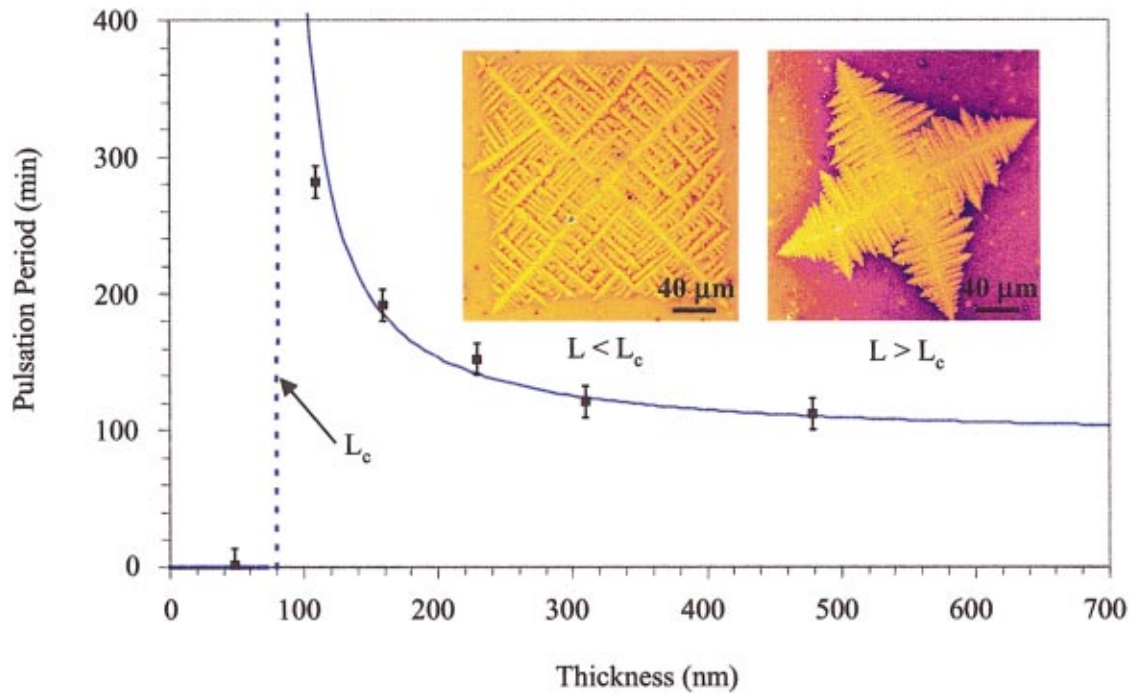


FIG. 6. (Color) Influence of film thickness on period P of growth oscillations. We find a sharp rise of P as the film becomes thinner and P then drops to zero below a critical thickness $L_c \approx 80$ nm. The right and left inset figures show the dendritic growth pattern for $L = 50 \text{ nm} < L_c$ and $L = 160 \text{ nm} > L_c$, respectively. L_c is the fitted value of the “critical film thickness” at which the pulsing period diverges. The correlation coefficient for the exponential fit is $R^2 = 0.98$. We see no pulsation in near “two-dimensional” films ($L = 50 \text{ nm} < L_c$).

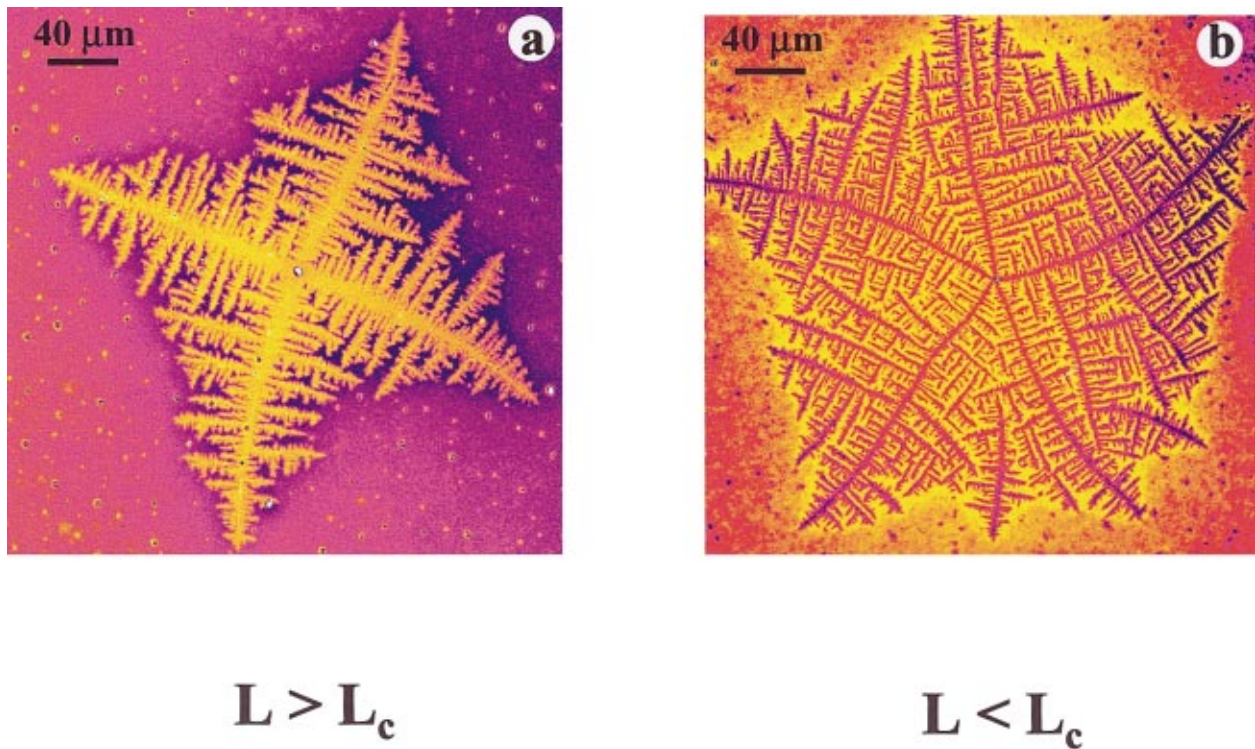


FIG. 7. (Color) Spiraling of dendrite arms at high clay concentrations. Clay concentration is 15% by relative mass to polymer, compared to 5% in Fig. 2(a). (a) The competition between the clay sources apparently causes the dendrite arms to spiral. Film thickness $L = 160$ nm. Note also the tapering of the width of the dendrite arms away from the center of the dendrite. (b) In the thinner, near two-dimensional films ($L = 160$ nm) we observe more space filling and disordered dendritic growth. Observe the near fivefold symmetry of the dendrite. Dendrites with larger numbers of arms are also observed at these high clay concentrations.

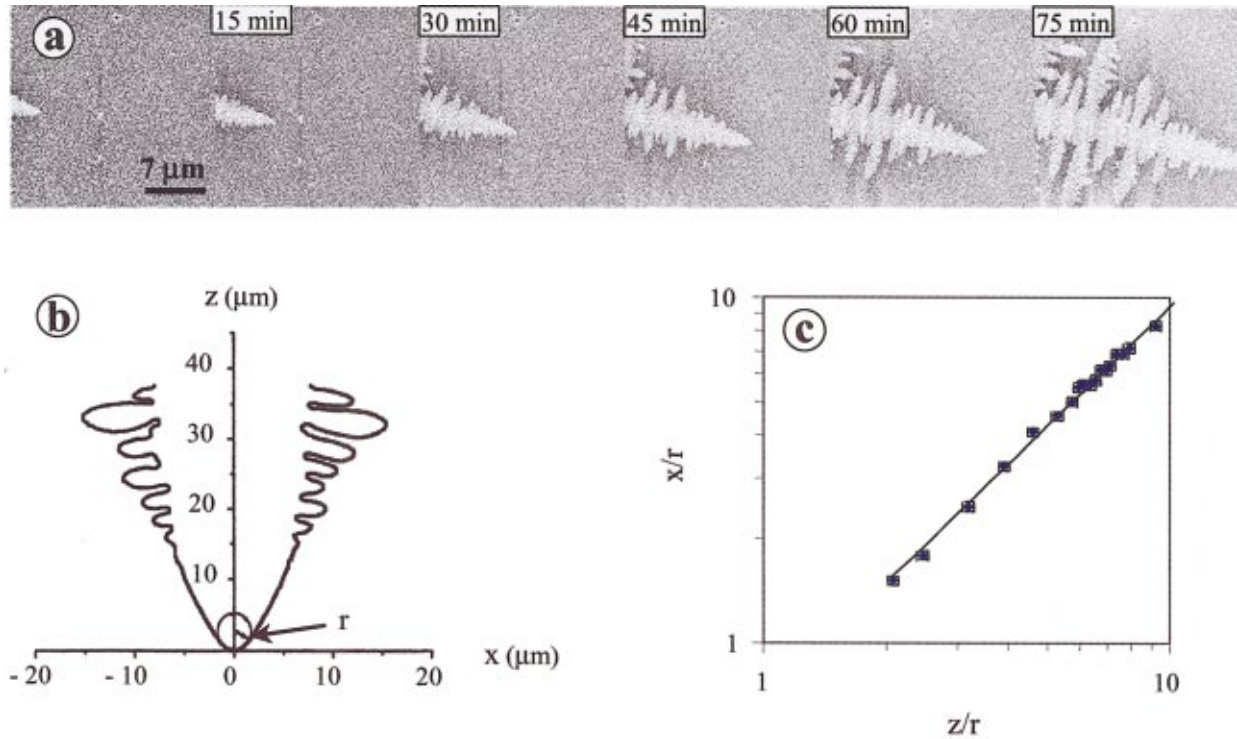


FIG. 8. (Color) The average shape of the dendrite trunk. (a) AFM images of a growing polymer dendrite corresponding to a thickness ($L = 50$ nm) where there are no growth pulsations. The pixel resolution for these AFM pictures is 40 nm. (b) Schematic indication of the coordinate system used for measuring the average shape of the dendrite trunk (schematic image corresponds to rotated contour of a xenon dendrite [22] with modified spatial scales). The position of the trunk growth tip is chosen to be the origin of our coordinate system, z is the distance away from the tip along the dendrite axis, and x is the distance normal from the dendrite axis. The average shape of the dendrite trunk is obtained by measuring the locus of points swept out by the sidebranch tips as they grow. z and x are coordinates of the sidebranch tip positions as a function of time for the sidebranches indicated in (a). (c) Log-log plot of x and z sidebranch tip coordinates normalized by the trunk tip radius r .

tallization for a high concentration of filler particle nucleation sites. Figure 7(a) shows a 160 nm film of a 30/70 relative composition PEO/PMMA blend films with a 15% relative mass clay filler concentration in the spin-casting solution. We indeed observe a tendency for the dendrite arms to rotate about the dendrite core in a vortexlike fashion at large filler concentrations. This spontaneous symmetry breaking arises from the disordering effect of the clay.

The growth pulsations also have a striking influence on the crystallization morphology at high clay concentrations. In Fig. 7(b) we consider the same composition film as Fig. 7(a), but having a thickness in the range ($L \approx 50$ nm) where growth pulsations are suppressed (see Fig. 6). The dendrites formed in the nearly two-dimensional film with a high clay concentration are more space filling and disordered in form. Note also the noncrystallographic branching habit, which is another characteristic feature that emerges from the disorder caused by the high clay concentration.

VI. THE AVERAGE SHAPE OF THE DENDRITE TRUNKS

Many recent studies of SDC crystallization have emphasized the shape of the dendrite in the immediate vicinity of the tip of the growing dendrite arm trunks and the shape of the average envelope curve describing the tip positions of the sidebranches growing off the trunk. These quantities are con-

sidered here for our polymer crystallization measurements because they are relevant to our discussion of the origin of the tip and sidebranch oscillations in Sec. VII. We utilize a high-resolution technique (AFM) for this measurement.

Figure 8(a) shows a series of AFM images of a growing polymer dendrite corresponding to a thickness ($L = 50$ nm) where there are no growth pulsations. Time is indicated as an inset in the figure. The scale of the AFM images is 20×20 (μm)² and the inset to Fig. 2(c) corresponds to this same growth series and to the time $t = 50$ min. In the inset to Fig. 2(a) we show a corresponding AFM image for a pulsating dendrite under the same growth conditions, except for the film thickness ($L = 160$ nm).

The tip radius in both the pulsating and nonpulsating dendrites remains nearly parabolic and has a tip radius, $r \approx 1$ μm. We can determine the average shape of the dendrite arm by measuring the locus of points swept out by the dendrite tips as they grow. Figure 8(b) shows a schematic indication of the coordinate system used. An arbitrary sidebranch was utilized for this measurement. The position of the dendrite tip is chosen to be the origin of our coordinate system, z is the distance away from the tip along the dendrite axis, and x is the distance normal from the dendrite axis. In Fig. 8(c), we show our observations for the z and x coordinates of the sidebranch tip positions normalized by the tip radius r .

The average shape of the dendrite tip is found to closely approximate a power law, $z/r \sim (x/r)^\beta$, where $\beta = 1.8 \pm 0.04$. The correlation coefficient for the data points fit $R^2 = 0.99$. A similar scaling relation has been found for the growth of the tip shape envelope in succinonitrile dendrites in three dimensions, but with a different prefactor and exponent [56]. The measurement of the sidebranch width x shows oscillations in thick films ($L > 80$ nm) so this type of analysis is not possible unless we determine the mean tip width where the oscillations about the mean have been subtracted. We do not consider these more complicated measurements here.

VII. DISCUSSION

A. Growth pulsations

There have been previous measurements indicating the presence of growth pulsations in nonequilibrium crystallization. In the earliest report, Morris and Winegard [57] showed images of dendritic crystallization in a directional solidification of succinonitrile with 5% (relative mass) camphor added, which indicated a tendency of the growing dendrite tip of the main dendrite arms to flatten and then to grow symmetric sidebranches. This work was followed by similar brief observations on the dendritic crystallization NH_4Cl in aqueous solutions and in the crystallization of nearly pure ^3He solutions [58,59]. Sawada *et al.* [60] first quantified the type of dendrite growth oscillation seen by Morris and Winegard. They found an oscillation in the dendrite trunk tip radius and trunk tip radius of curvature for free-standing dendrites grown from a succinonitrile solution with 8% relative mass acetone. Interestingly, the time periods of fluctuations of the tip growth and decay are asymmetric and the total period of the tip growth pulsations decrease with undercooling in these measurements. Sawada *et al.* [60] proposed that the oscillatory dendritic growth arises from a competition between the surface tension and kinetic anisotropies, but this explanation remains speculative.

The observations of Sawada *et al.* are contrasted with our own measurements of growth oscillations in polymer-blend films that indicate that the sidebranches are emitted from the sides of the leading parabolic tip so that the radius of dendrite tip radius has no discernable time dependence (by optical microscopy). We also find that the width of a representative sidebranch oscillates out of phase with the propagating tip, forming a limit cycle. Our findings are apparently more related to recent observations of a limit cycle dynamics in the directional solidification in pure succinonitrile [29]. In these measurements, the crystallization front forms an array of fingerlike “cells” near the pulling velocity where the growth front makes a transition to asymmetric doublet cell growth (a transition to dendritic front growth occurs at higher pulling velocities). The oscillations involve the tip position of the advancing cell, relative to the tip position of an adjacent cell and the relative width of these “excited” cells. Moreover, recent directional solidification measurements of succinonitrile (with PEO added to increase the viscosity and thus slow the crystallization kinetics) have indicated that the tip splitting of the seaweed dendritic growth occurs as an oscillatory mode between the predominant

growth of the right and left branch tips [61]. The dendrite arm then has a varicose mode of oscillatory growth that resembles a “swimming” (crawl) of the tip into the surrounding medium. For our symmetric polymer dendritic growth, we rather observe a symmetric pulsation mode of dendrite tip growth. These complementary observations point to the importance of a tip-branching dynamics governed by global hydrodynamic modes. Moreover, the change of dendrite morphology evidenced by our thin-film measurements indicates that these hydrodynamic sidebranching modes can significantly impact the dendrite morphology. Thus, many aspects of the growth morphology are encoded in the nature of the excited modes of the crystallization front.

The presence of hydrodynamic front propagation modes potentially offers significant opportunities for controlling the crystallization morphology through exciting these modes with applied fields. Early measurements showed that an oscillatory flow field can regularize the structure of dendritic growth in pivalic acid/ethanol mixtures [62] and measurements have also shown that pulsating dendritic growth can be stimulated by periodic local heating of the dendrite tip with a pulsed laser beam [50]. Both the simulation and the experiment have recently shown that pulsating symmetric dendritic growth (coherent sidebranching and tip oscillations) can be stimulated nonlocal imposed oscillations of the fluid pressure and temperature, thereby exerting a significant control on the resulting crystallization morphology [51]. It would be interesting to explore this mode of controlling crystallization morphology in polymer crystallization.

The finding of coherent sidebranching and tip position oscillations in polymer dendritic crystallization in polymer films naturally leads to questions about whether similar oscillatory modes arise in the important case of spherulitic polymer crystallization. There have indeed been recent reports of radial growth oscillations in spherulitic polymer crystallization in a polymer blend, both by phase field simulation [63] and experiments [63–65]. (Note the simulation in [63] does not incorporate surface tension anisotropy and thermal transport and thus generates circular propagating crystallization fronts.) Future work should focus on whether stress oscillations occur in the amorphous medium surrounding the growing dendrites and on how the character of the growth pulsations changes with growth morphology and influence interdendrite interactions.

It should be appreciated that although our polymer-blend films are thin enough to be idealized as being “two-dimensional” for comparison with simulations of two-dimensional dendritic growth, this point of view does not account for the transfer of the latent heat of crystallization to the Si wafer substrate. Both the theory and the experiment have shown that the heat transfer from the film to the substrate can lead to the formation of self-sustaining oscillatory crystallization waves by perturbing these films with a laser or mechanically by scratching or piercing [66,67]. (If the substrate draws away the heat of fusion too rapidly then the film crystallization stops so that the temperature of the substrate is important in this type of film crystallization.) The proposed mechanism [66,67] of the growth front oscillations in “explosive film crystallization” is the strong temperature de-

pendence of the crystallization rate that makes the diffusion equation for the latent heat of crystallization highly nonlinear. The basic physical origin of the effect is that the liberation of latent heat at the crystallization front allows the front to advance rapidly, but the material behind the front cannot keep up and the crystal growth then slows down until more heat can diffuse to the boundary. Kurtze, van Saarloos, and Weeks [68] argue that this mechanism is not operative in dendritic crystallization growth in thin films and, moreover, this pulsation scenario should be accompanied by a series of period doublings in the growth front oscillations [67,68] (an effect that we do not observe). Polymer materials and many other organic fluids often have viscosity and polymer diffusion coefficients that depends strongly on temperature (i.e., “fragile” liquids) so that the release of the heat of crystallization can be expected to lead to large mobility changes and thus to large changes in the local rate of crystallization. This effect should be true regardless of the morphology of the polymer, but its influence should be sensitive to the film geometry since the rate of heat removal by the boundaries would modulate the intensity of this effect. The mode coupling between compositional and heat transport in the fluid caused by the asymmetries of mass and thermal transport coefficients and the strong temperature dependence of the transport properties must also be considered as a possible candidate for the growth oscillations in our films. Growth oscillations of this kind have been observed and theoretically modeled in the case of propagating combustion fronts in burning fuels [69]. It is possible that the oscillations associated with this type of transport coupling are amplified by the sidebranches in much the same way as dendrites are “regularized” by applied external fields. This possibility for the origin of dendritic pulsations suggests that we vary the heat transfer from the film to the boundary to see how this might influence dendritic tip pulsations.

There are numerous other possible causes of growth pulsations, including the transient buildup of stress on the advancing tip of the crystallization front, the non-Newtonian character of the polymer film, intrinsic oscillations related to the dynamics of crystallization as in the geometrical model [23], accumulation of impurities at the growth front associated with residual solvent within the film, coupling between phase separation and crystallization dynamics, etc. All these possibilities require further measurements to unequivocally assign the origin of the growth pulsations in our measurements.

Regardless of the particular mechanism of the growth oscillations, however, we have shown that the structure of symmetric dendrites is not generally governed by the amplification of thermal noise as some experiments have previously suggested. Many naturally occurring dendrites (e.g., snowflakes) exhibit a highly correlated sidebranch structure similar to our dendrites grown under conditions of growth pulsations so that we believe growth pulsations are ubiquitous, even if their cause is not universal.

B. Dendritic crystallization and autocatalytic chemical reactions

The similarities between the growth dynamics of dendritic crystallization and wave propagation in autocatalytic chemi-

cal reactions suggest a useful viewpoint of crystallization under nonequilibrium conditions. It seems reasonable to consider a highly supercooled liquid to be a variety of an “excitable medium” [70] so that the crystallization front corresponds to a propagating wave [3] in this (nonregenerative) medium. The constant average rate of propagation of the crystallization front is a basic property of reaction-diffusion wave propagation [71] and pulsations are commonly associated with these propagating fronts [72]. From this point of view, the observation of wavelike growth of crystallization patterns, growth pulsations, finite-size effects on the pulsation period and spontaneous symmetry breaking of the growth pattern shape with disorder is “obvious.” Notably, nonlinear wave propagation into an excitable medium is found in many other physical contexts (growth of cell colonies [73,74], replication of RNA [75], propagating flame fronts in burning fuels [69], chemical waves, such as the BZ reaction [76], waves of polymerization [77], tubulin formation [78], spread of a fluid front into a porous medium or a more viscous fluid [79], catalyzed chemical reactions on surfaces [80], self-propagating synthesis of ceramics and metallic blends (thermites) [81], waves of excitation in cellular populations [82], nerve propagation [83], spread of infectious diseases or advantageous genes through a population of living organisms [84–86], crack propagation in polymers [87], film dewetting [88], etc.) and there are often striking similarities between the patterns in these many nonequilibrium pattern formation processes and those found in nonequilibrium crystallization (densely branched “spherulites” resembling the crystallization of exotic and rare minerals, “seaweed” crystals resembling natural growth forms in living systems, “symmetric dendrites” with similarities to snowflakes, and “fractal dendrites” resembling colloid particle aggregates [19,31,73]).

We mentioned already that recent experiments and simulation have suggested the presence of oscillations in the radial growth of “ringed” polymer spherulites [63,64]. These growth patterns strongly resemble BZ target reaction-diffusion patterns in form and it would be interesting to add filler particles to these materials to determine if we can induce a transition between the circular and spiral growth patterns in spherulitic polymer crystallization. Spiral crystallization patterns have been observed in polymeric materials [64], although it is not clear that heterogeneities are the cause of this phenomenon.

C. Summary

The dynamics of the growing tips of crystals forming under conditions far from equilibrium has a large impact on the resulting crystal morphology and thus the material properties of “semicrystalline” materials. Undulating modes have been identified in seaweed-type crystallization in succinonitrile [61] and the present measurements provide clear evidence for a limit cycle dynamics in the dendritic growth of PEO in a crystalline/amorphous polymer-blend films. Previous measurements of directional solidification in succinonitrile have also provided evidence of growth (arm tip and width) oscillations of crystallization cells near the symmetric cell to

asymmetric doublet cell transition [28,29]. These observations, along with our own, point to the importance of tip hydrodynamic modes in influencing the morphology of dendritic growth. Notably, the finite-size dependence of the tip pulsation period in our measurements is similar to those found in BZ reactions occurring in gel beads. We also observe a tendency for the arms of the crystallization patterns to rotate at high clay concentrations, which is analogous to spiral formation in the BZ reaction with interfering sources. With this hindsight, we can consider polymer crystallization to be a variety of autocatalytic reaction (uncrystallized polymer “reacting” with crystallized polymer to form more crystallized polymer “products”). In this view, the growing dendrite is the propagating wave of an autocatalytic wave where the amorphous medium is the “excitable” medium. We found this point of view helpful in interpreting qualitative properties of symmetric dendrite formation, and this analogy stimulated many of the measurements described in our paper, such as the investigation of how a high clay concentration influences dendrite morphology. This “analogy” also has strong implications about the rate of crystallization (“wave propagation”) in relation to the diffusion coefficient of the crystallizing species that remains to be checked [89].

Many physical effects can lead to oscillations in the velocity of propagating nonequilibrium growth fronts and further experiments and simulations are necessary to resolve their origin in our blend film measurements. Nonetheless, the present measurements prove that growth pulsations can occur spontaneously in free symmetric dendritic growth accompanied by coherent and periodic emission of side-branches and that these hydrodynamic modes in the growth front can have a large impact on the regularity of the crystallization morphology.

Note added in proof. Recently, we became aware of growth pulsations similar to Fig. 2 in the spherulitic growth of poly(methylene) oxide films (≈ 20 m thick) between glass plates [90]. This work attributes the pulsations to convective flow in the melt induced by pressure fluctuations in the confined crystallizing polymer films.

ACKNOWLEDGMENTS

The authors are very grateful to Bernard Lotz (ICS, Strasbourg, France) for helpful discussions. We also thank Ronald Heddon and Charles Guttman of the Polymers Division at NIST for characterizing the polydispersity of our PEO and PMMA samples by gel permeation chromatography.

-
- [1] B. Billia and R. Trivedi, in *Handbook of Crystal Growth*, edited by D. T. J. Hurle (Elsevier, Amsterdam, 1993), Vol. 1, Chap. 14; R. Trivedi and W. Kurz, *Int. Mater. Rev.* **39**, 49 (1994).
- [2] B. Wunderlich, *Macromolecular Physics* (Academic, New York, 1973–1980), Vols. 1–3.
- [3] E. Ben-Jacob, *Contemp. Phys.* **34**, 247 (1993).
- [4] W. W. Mullins and R. W. Sekerka, *J. Appl. Phys.* **34**, 323 (1963).
- [5] W. W. Mullins and R. W. Sekerka, *J. Appl. Phys.* **35**, 444 (1964).
- [6] B. J. Johnson and R. W. Sekerka, *Phys. Rev. E* **52**, 6404 (1995).
- [7] J. S. Langer, *Science* **243**, 1150 (1989).
- [8] M. Ben Amar and Y. Pomeau, *Europhys. Lett.* **2**, 307 (1986).
- [9] S. Akamatsu, O. Bouloussa, K. To, and F. Rondolez, *Phys. Rev. A* **46**, R4504 (1992).
- [10] P. Oswald, *J. Phys. (France)* **49**, 1083 (1988).
- [11] D. A. Kessler, J. Koplik, and H. Levine, *Phys. Rev. A* **30**, 3161 (1984).
- [12] Y. Sawada, B. Perrin, P. Tabeling, and P. Bouissou, *Phys. Rev. A* **43**, 5537 (1991).
- [13] J. H. Magill and D. J. Plazek, *J. Chem. Phys.* **46**, 3757 (1967). Nearly two-dimensional spherulites have been observed to grow in highly viscous glucose solutions [A. S. Parajpe, *Phys. Lett. A* **176**, 349 (1993)].
- [14] A. Keller and J. R. S. Waring, *J. Polym. Sci.* **17**, 447 (1955).
- [15] H. D. Keith and F. J. Padden, Jr., *J. Appl. Phys.* **34**, 2409 (1963).
- [16] H. D. Keith and F. J. Padden, Jr., *J. Appl. Phys.* **35**, 1286 (1964).
- [17] V. Fleury, J. H. Kaufman, and D. B. Hibbert, *Nature (London)* **367**, 435 (1994). These measurements indicate that convection plays a large role in the growth of electrochemical “spherulites” and this effect illustrates a *reactive response* of the growth medium to the incursion of the growing crystal. The regular needlelike crystals form due to the large fluctuations in the surrounding medium that suppress tip splitting. Spherulites tend to form from *viscous* polymer melts and this phenomenology suggests that the growth of the polymer may induce a stress field that reacts upon the growing needles of the polymer spherulites. The stress field surrounding the growing dendrites should then be examined experimentally in a fashion similar to the electrochemical measurements. See R. M. Suter and P. Wong, *Phys. Rev. B* **39**, 4536 (1989) and C. Livermore and P. Wong, *Phys. Rev. Lett.* **72**, 3847 (1994).
- [18] E. Brener, H. Levine, and Y. H. Tu, *Phys. Rev. Lett.* **15**, 1978 (1991). It has been suggested that spherulites correspond to a highly branched variety of seaweed [N. Goldenfeld, *J. Cryst. Growth* **84**, 601 (1987)].
- [19] T. Ihle and H. Müller-Krumbhaar, *Phys. Rev. E* **49**, 2972 (1994); E. Brener, H. Müller-Krumbhaar, and D. Temkin, *ibid.* **54**, 2714 (1996); E. Brener, H. Müller-Krumbhaar, D. Temkin, and T. Abel, *Physica A* **249**, 73 (1998).
- [20] J. S. Langer, *Rev. Mod. Phys.* **52**, 1 (1980).
- [21] A. Dougherty, P. D. Kaplan, and J. P. Kaplan, *Phys. Rev. Lett.* **58**, 1652 (1987).
- [22] U. Bisang and J. H. Bilgram, *Phys. Rev. E* **54**, 5309 (1996).
- [23] D. Kessler, J. Koplik, and H. Levine, *Phys. Rev. A* **30**, 3161 (1984).
- [24] O. Martin and N. Goldenfeld, *Phys. Rev. A* **35**, 1382 (1987); see also D. A. Kessler and H. Levine, *Europhys. Lett.* **4**, 215 (1987).
- [25] R. Pieters and J. S. Langer, *Phys. Rev. Lett.* **56**, 1948 (1986).

- [26] J. Nittmann and E. Stanley, *J. Phys. A* **20**, L-981 (1987).
- [27] A. Karma and P. P. Pelcé, *Phys. Rev. A* **39**, 4162 (1989).
- [28] M. Georgelin and A. Pocheau, *Phys. Rev. E* **57**, 3189 (1998).
- [29] M. Georgelin and A. Pocheau, *Phys. Rev. Lett.* **79**, 2698 (1997).
- [30] L. Sung, A. Karim, J. F. Douglas, and C. C. Han, *Phys. Rev. Lett.* **76**, 4368 (1996); B. D. Ermi, A. Karim, and J. F. Douglas, *J. Polym. Sci. Part B: Polym. Phys.* **36**, 191 (1998).
- [31] V. Ferreiro, J. F. Douglas, J. A. Warren, and A. Karim, *Phys. Rev. E* (to be published). See Ref. [38] for a preliminary report of our polymer crystallization measurements and data relating to the crystallization and melting temperatures and glass transition temperatures of our PMMA/PEO blends as a function of relative mass composition. Tóth-Katona *et al.* [*Phys. Rev. E* **54**, 1574 (1996)] considered mixtures of liquid crystal forming liquids having very different ε values and found large morphological changes in the resulting crystallization pattern. At least part of these changes can be attributed to the change of the effective value ε for these mixtures.
- [32] Certain commercial materials and equipment are identified in this paper in order to specify adequately the experimental procedure. In no case does such an identification imply recommendation by the NIST, nor does it imply that the material or equipment identified is necessarily the best available for this purpose. According to ISO 31-8 the term “molecular weight” has been replaced by relative molecular mass M_r , so that the number average relative molecular mass equals $M_{r,n}$.
- [33] G. C. Alfonso and T. P. Russel, *Macromolecules* **19**, 1143 (1986); E. Martuscelli, M. Pracella, and W. P. Yue, *Polymer* **25**, 1097 (1984).
- [34] M. Cortazar, M. E. Calahorra, and G. M. Guzman, *Eur. Polym. J.* **18**, 165 (1982).
- [35] S. A. Liberman, A. D. S. Gomes, and E. M. Macchi, *J. Polym. Sci., Polym. Chem. Ed.* **22**, 2809 (1984).
- [36] S. Cimmino, E. Martuscelli, and C. Silvester, *Polymer* **30**, 393 (1989).
- [37] A. C. Fernandes, J. W. Barlow, and D. R. Paul, *J. Appl. Polym. Sci.* **32**, 5481 (1986); K. E. Min, J. S. Chiou, J. W. Barlow, and D. R. Paul, *Polymer* **28**, 1721 (1987).
- [38] V. Ferreiro, J. F. Douglas, E. J. Amis, and A. Karim, *Macromol. Symp.* **167**, 73 (2001). The molecular mass values reported in this paper correspond to supplier values estimated from intrinsic viscosity measurements. The present paper provides more accurate estimates based on gel permeation chromatography.
- [39] A. B. Burdin and A. A. Tager, *Ysol. Soed. Ser. B* **37**, 850 (1995). The effect of solvent retention on the dynamics of PMMA films is discussed by S. Bistac and J. Schultz [*Prog. Org. Coat.* **31**, 347 (1997)].
- [40] J. W. Cahn, *J. Am. Ceram. Soc.* **52**, 118 (1969).
- [41] DI Digital Instruments, Dimension 3100, Scanning Probe Microscopes, Instruction Manual, Digital Instruments, Santa Barbara, CA.
- [42] D. Weaire and N. Rivier, *Contemp. Phys.* **25**, 59 (1984).
- [43] J. Chen, S. Z. D. Cheng, S. S. Wu, and B. Lotz, *J. Polym. Sci., Part B: Polym. Phys.* **33**, 1851 (1995); A. J. Kovacs, B. Lotz, and A. Keller, *J. Macromol. Sci., Phys.* **B3**, 385 (1969). The crystal lattice of PEO is monoclinic and the chain conformation has been identified as a $\frac{7}{2}$ helix.
- [44] P. H. Till, *J. Polym. Sci.* **24**, 301 (1957); H. D. Keith and F. J. Padden, *ibid.* **39**, 123 (1959). The dendrite crystals of polyoxymethylene grown from orthodichlorobenzene solutions have been observed to grow in a curved form resembling a flower [F. Khoury and J. D. Barnes, *J. Res. Natl. Bur. Stand., Sect. A* **78A**, 95 (1974)]. Unusual seaweed dendrites have been observed to grow from melts of poly(trifluoroethylene) [A. Lovinger and R. A. Cais, *Macromolecules* **17**, 1939 (1984)].
- [45] D. Braun, M. Jacobs, and G. P. Hellmann, *Polymer* **35**, 706 (1994). This reference is only illustrative of a large literature.
- [46] M. E. Glicksman, R. J. S. Schaefer, and J. D. Ayers, *Metall. Trans. A* **7A**, 1747 (1976).
- [47] J. A. Warren and W. J. Boettinger, *Acta Metall. Mater.* **43**, 689 (1995); A. A. Wheeler, W. J. Boettinger, and G. B. Mc Fadden, *Phys. Rev. A* **45**, 7424 (1992); M. Rappaz and W. Kurz, *Nature (London)* **375**, 103 (1995); see also A. Karma and W.-J. Rappel, *Phys. Rev. E* **57**, 4323 (1998).
- [48] S. Lovejoy, *Science* **216**, 185 (1982); S. N. Rauser, P. D. Barnes, and J. V. Maher, *Phys. Rev. A* **35**, 1245 (1987).
- [49] M. E. Glicksman and S. P. Marsh, in *Handbook of Crystal Growth* (Ref. [1]), Chap. 15.
- [50] X. Qian and H. Z. Cummins, *Phys. Rev. Lett.* **64**, 3038 (1990); L. Williams, M. Muschol, X. Qian, W. Losert, and H. Z. Cummins, *Phys. Rev. E* **48**, 489 (1993); B. T. Murray, A. A. Wheeler, and M. E. Glicksman, *J. Cryst. Growth* **154**, 386 (1995).
- [51] T. Börzönyi, T. Tóth-Katona, Á. Buka, and L. Gránásy, *Phys. Rev. Lett.* **83**, 2853 (1999); *Phys. Rev. E* **62**, 7817 (2000).
- [52] K. Yoshikawa, R. Aihara, and K. Agladze, *J. Phys. Chem. A* **102**, 7659 (1998); R. Aliev and K. Agladze [*Physica D* **50**, 65 (1991)] observed that a critical layer thickness was required for the propagation of BZ reaction waves.
- [53] J. Maselko, J. S. Reckley, and K. Showalter, *J. Phys. Chem.* **93**, 2774 (1989).
- [54] O. Steinbock, P. Kettunen, and K. Schowater, *Nature (London)* **269**, 1857 (1995).
- [55] G. Weidemann and D. Vollhardt, *Biophys. J.* **70**, 2758 (1996).
- [56] Q. Li and C. Beckmann, *Phys. Rev. E* **57**, 3176 (1998). The measurements were made under microgravity conditions by Glickman *et al.*, *Phys. Rev. Lett.* **73**, 573 (1993).
- [57] L. R. Morris and W. C. Winegard, *J. Cryst. Growth* **1**, 245 (1967).
- [58] H. Honjo, S. Ohta, and Y. Sawada, *Phys. Rev. Lett.* **55**, 841 (1985).
- [59] E. Rolley, S. Ballibar, and F. Gallet, *Europhys. Lett.* **2**, 247 (1986).
- [60] Y. Sawada, B. Perrin, P. Tabeling, and P. Boussou, *Phys. Rev. A* **43**, 5537 (1991).
- [61] B. Utter, R. Ragnarsson, and E. Bodenschatz, *Phys. Rev. Lett.* **86**, 4604 (2001).
- [62] Ph. Bouissou, A. Chiffandel, B. Perrin, and P. Tabeling, *Europhys. Lett.* **13**, 89 (1990).
- [63] T. Kyu, H.-W. Chiu, A. J. Guenther, Y. Okabe, H. Sato, and T. Inoue, *Phys. Rev. Lett.* **83**, 2749 (1999).
- [64] Y. Okabe, T. Kyu, H. Sato, and T. Inoue, *Macromolecules* **31**, 5823 (1998).
- [65] Z. Wang, L. An, B. Jiang, and X. Wang, *Macromol. Rapid Commun.* **19**, 131 (1998).
- [66] W. van Saarloos and J. D. Weeks, *Phys. Rev. Lett.* **51**, 1046

- (1983); *Physica D* **12**, 279 (1984).
- [67] C. E. Wickersham, G. Bajor, and J. E. Greene, *Solid State Commun.* **27**, 17 (1978).
- [68] D. A. Kurtze, W. van Saarloos, and J. F. Weeks, *Phys. Rev. B* **30**, 1398 (1984).
- [69] B. J. Matowsky and G. I. Sivashinsky, *SIAM (Soc. Ind. Appl. Math.) J. Appl. Math.* **35**, 465 (1978); Y. Zeldovich, A. G. Istratov, N. I. Kidin, and V. B. Librovich, *Combust. Sci. Technol.* **24**, 1 (1980).
- [70] A. T. Winfree, *SIAM Rev.* **32**, 1 (1990); I. E. Epstein and K. Showalter, *J. Phys. Chem.* **100**, 13 132 (1996).
- [71] P. C. Fife and J. B. McLeod, *Bull. Am. Math. Soc.* **81**, 1076 (1975); J. H. Merkin and D. J. Needham, *J. Eng. Math.* **23**, 343 (1989).
- [72] P. Kaliappan, *Physica D* **11**, 368 (1984); C. B. Muratov and V. V. Osipov, *Phys. Rev. E* **53**, 3101 (1996); K. Kærn and M. Menzinger, *ibid.* **61**, 3334 (2000).
- [73] E. Ben-Jacob and P. Garik, *Nature (London)* **343**, 523 (1990); E. Ben-Jacob, H. Shmueli, O. Shochet, and A. Tenebaum, *Physica A* **187**, 378 (1992); E. Ben-Jacob, O. Shochet, A. Tenebaum, I. Cohen, A. Czirók, and T. Vicsek, *Nature (London)* **368**, 46 (1994); E. Ben-Jacob, O. Shochet, A. Tenebaum, I. Cohen, A. Czirók, and T. Vicsek, *Fractals* **2**, 15 (1994).
- [74] A. Nakahara, Y. Shimada, J. Wakita, M. Matsushita, and T. Matsuyama, *J. Phys. Soc. Jpn.* **65**, 2700 (1996); A. Czirók, M. Matsushita, and T. Vicsek, *Phys. Rev. E* **63**, 031915 (2001).
- [75] G. J. Bauer, J. S. McCaskill, and H. Otten, *Proc. Natl. Acad. Sci. U.S.A.* **86**, 7937 (1989); J. S. McCaskill and G. J. Bauer, *ibid.* **90**, 4191 (1993).
- [76] J. Ross, S. C. Miller, and C. Vidal, *Science* **240**, 460 (1988); R. Yoshida, E. Kokufuta, and T. Yamaguchi, *Chaos* **9**, 260 (1999).
- [77] J. A. Pojman, V. M. Ilyashenko, and A. M. Khan, *J. Chem. Soc., Faraday Trans.* **92**, 2825 (1996); S. E. Solovyov, V. M. Ilyashenko, and J. A. Pojman, *Chaos* **7**, 331 (1997); R. Sambeth and A. Baumgaertner, *Phys. Rev. Lett.* **86**, 5196 (2001).
- [78] E. Mandelkow, E. Mandelkow, H. Hotani, B. Hess, and S. C. Miller, *Science* **246**, 1291 (1989); E. Mandelkow and E. Mandelkow, *Cell Motil. Cytoskeleton* **22**, 235 (1992); A. S. Bajer, *J. Cell Biol.* **93**, 33 (1982).
- [79] P. G. Saffman and G. I. Taylor, *Proc. R. Soc. London, Ser. A* **245**, 312 (1958); K. V. McCloud and J. V. Maher, *Phys. Rep.* **260**, 139 (1995); L. Kondic, M. J. Shelley, and P. Palffy-Muhoray, *Phys. Rev. Lett.* **80**, 1433 (1998).
- [80] G. Ertyl, *Science* **254**, 1750 (1991).
- [81] U. Anselm-Tamburini and Z. A. Munir, *J. Appl. Phys.* **66**, 5039 (1989).
- [82] O. Steinbock, F. Siegert, S. C. Miller, and C. J. Weijer, *Proc. Natl. Acad. Sci. U.S.A.* **90**, 7332 (1993); K. J. Tomchik and P. N. Devreotes, *Science* **212**, 443 (1981).
- [83] A. L. Hodgkin and A. F. Huxley, *J. Physiol. (London)* **117**, 500 (1952); J. Nagumo, S. Arimoto, and S. Yoshizawa, *Proc. Inst. Radio Eng.* **50**, 2061 (1992); J. M. Davidenko, A. V. Pertsov, R. Salomonsz, W. Baxter, and J. Jalife, *Nature (London)* **355**, 349 (1992).
- [84] J. T. Gleeson, *Nature (London)* **385**, 511 (1997).
- [85] H. P. McKean, *Commun. Pure Appl. Math.* **28**, 323 (1975); R. A. Fisher, *Ann. Eug.* **7**, 355 (1936); A. I. Kolmogorov, I. Petrovskii, and N. Piskunov, *Moscow Univ. Bull. Math.* **1**, 1 (1937); see also Ref. [70].
- [86] Y. Lee and J. Yin, *Nat. Biotechnol.* **14**, 491 (1996); see also J. Yin and J. S. McCaskill, *Biophys. J.* **61**, 1540 (1992); J. Yin, *J. Bacteriol.* **175**, 1272 (1993); L. You and J. Yin, *J. Theor. Biol.* **200**, 365 (1999).
- [87] J. Fineberg, S. P. Gross, M. Marder, and H. L. Swinney, *Phys. Rev. Lett.* **67**, 457 (1991); see also D. A. Kessler and H. Levine, *Phys. Rev. E* **63**, 016118 (2001).
- [88] E. Brener, H. Müller-Krumbhaar, D. Temkin, and T. Abel, *Solid State Ionics* **131**, 22 (2000); R. Yerushalmi-Rozen, T. Kerle, and J. Klein, *Science* **285**, 1254 (1999); O. Karthaus, L. Gåsjö, N. Maruyama, and M. Shimomura, *Chaos* **9**, 308 (1999); X. Gu, D. Raghavan, J. F. Douglas, and A. Karim (unpublished).
- [89] K. Showalter and J. J. Tyson, *J. Chem. Educ.* **64**, 742 (1987); L. Kuhnert, H.-J. Krug, and L. Pohlmann, *J. Phys. Chem.* **89**, 2022 (1985).
- [90] A. Pawlak and A. Galeski, *J. Polym. Sci., Part B: Polym. Phys.* **28**, 1813 (1990).